Analysis of Two-Phase Flow Processes in Rocket Exhaust Plumes

S. M. Dash,* D. E. Wolf,† R. A. Beddini,‡ and H. S. Pergament§
Science Applications, Inc., Princeton, New Jersey

An overview is given of the coupled two-phase flow processes occurring in rocket exhaust plumes, and modeling procedures developed to treat these processes are surveyed. The full spectrum of particle size groups encountered is modeled by a hybrid partially equilibrated mixture approach, whereby a portion of the particulates is treated via nonequilibrium techniques. The influence of particulates on Mach disk locations and the treatment of particulate relaxation and turbulent mixing behind Mach disks is discussed in detail. A preliminary approach for treating the turbulent dispersion of particulates is presented which relates the particle diffusivity to that of the gas phase via local time scale relations. This approach is assessed via comparisons with available data extracted from the Russian literature.

Nomenclature

a = sound speed
$\bar{C}_D$ = particle drag coefficient scaled to Stokes' flow value
C_P = specific heat capacity
C_S = particle heat capacity
C_t = turbulence time scale constant
F = characteristic source term
h = static enthalpy
H = total enthalpy
k = turbulent kinetic energy
M = Mach number
M_j = lag Mach number based on $|\bar{Q}-\bar{Q}_p|$
$\bar{N}u$ = particle Nusselt number scaled to Stokes flow value
P = pressure
Pr = laminar Prandtl number
$\bar{Q}$ = velocity vector
Re_j = lag Reynolds number based on $|\bar{Q}-\bar{Q}_p|$
R_0 = universal gas constant
r_j = radius of jth particle size group
r_J = nozzle exit radius
r_p = particle radius
T = temperature
t = time scale
u_j, v_j = axial and radial particle velocities
U, V = axial and radial gas/mixture velocities
W = molecular weight
x, r = cylindrical coordinates
α = species mass fraction
γ = specific heat ratio
ϵ = turbulent dissipation parameter
θ = flow angle
κ = particle loading parameter
μ = Mach angle
$\tilde{\mu}$ = laminar viscosity
ν = turbulent diffusivity
ρ = gas/mixture density
ρ_j = particle cloud density
ρ_s = particle material density
σ = turbulent Prandtl number
τ = particle equilibration time
ϕ = mass fraction of equilibrated particles
$\dot{\omega}$ = chemical production term

Subscripts

i = chemical species; $i = 1, 2, \ldots, NS$
j = particle size group; $j = 1, 2, \ldots, NP$
J = jet radius at nozzle exit; (superscript denotes planar/cylindrical flow parameter; = 0, planar, = 1, cylindrical)
G = gas phase
M = equilibrated mixture
p = particle phase

Presented as Paper 83-0248 at the AIAA 21st Aerospace Sciences Meeting, Reno, Nev. Jan. 10-13, 1983; submitted March 2, 1983; revision received March 3, 1984. Copyright © American Institute of Aeronautics and Astronautics, Inc., 1983. All rights reserved.

*Technical Director, Propulsion Gas Dynamics Division. Member AIAA.
†Research Scientist, Propulsion Gas Dynamics Division. Member AIAA.
‡Senior Research Scientist, Propulsion Gas Dynamics Division. Member AIAA.
§Division Manager, Propulsion Gas Dynamics Division.

Overview of Two-Phase Flow Processes in Rocket Plumes

Plume Characterization

ROCKET exhaust plumes are characterized by turbulent mixing and afterburning in a flow initially dominated by strong wave processes. The initially underexpanded exhaust equilibrates to ambient pressure via a sequence of expansion and compression waves which decay due to shock-/turbulence-/particle-induced viscous dissipation. Mixing and afterburning processes are initiated in the shear layer growing along the plume interface separating the exhaust and external flow (Fig. 1). Mixing processes are also initiated along the slipstream separating the hot, initially subsonic streamtube which has traversed the Mach disk from the remaining exhaust flow, which has traversed the weaker barrel and reflected shocks.

Source of Particles

Particles, formed from condensed combustion products of metallized fuels (viz. metal oxides such as Al_2O_3 in aluminized propellants) in the motor, can have loadings (mass flux particles/mass flux gas) in excess of 50%. Secondary sources of particles in the motor come from propellant stability additives and from ablation of the motor case. The particles can be well out of equilibrium at the nozzle exit plane due to lag effects caused by the rapid nozzle expansion process. Therefore, particle velocities will be less than those of the gas, while temperatures will be higher. The degree of nonequilibrium is dependent upon particle size; the larger particles exhibit more lag effects and are thus slower and hotter. The radial variation of the particle size distribution at the nozzle exit plane is also nonuniform due to lag effects.

The larger particles, being relatively unresponsive to the gas expansion process, remain concentrated in the vicinity of the axis while the smaller particles tend to expand with the gas. This results in a highly rotational gas phase exit plane distribution, with the high-temperature gas near the centerline.

Mean Flow Nonequilibrium in Plume

The particle lag processes occurring in the nozzle continue into the near-field plume exhaust. Relaxation lengths for gas/particle equilibration (for a significant range of particle sizes) are, typically, comparable to inviscid plume length scales; but near-field wave processes are abrupt and quite strong. Thus, the path to equilibration is repetitively disrupted by passages through strong gas phase discontinuities. For significant particle loadings, the near-field inviscid flow pattern can be substantially altered by gas/particle interactions, with wave processes being dampened due to the viscous dissipation associated with particle drag.

Two-Phase Mach Disk Region

A region of significant gas/particle nonequilibrium is the embedded subsonic zone behind the Mach disk. Gas phase temperatures immediately downstream of the disk are quite high and velocities quite low. Temperature differences between gas and particle phases can exceed 3000 K, while velocity differences can be on the order of 10,000 ft/s. For single-phase flows, the acceleration of the subsonic flow in the Mach disk streamtube to supersonic velocities is governed by the local pressure gradient and turbulent mixing processes. For two-phase flows, gas/particle interactions can initially provide a significant accelerative mechanism and thus appreciably alter the flowfield characteristics in this region. In addition, nonequilibrium phase change effects can occur as can, possibly, combustion effects for noninert particulates (e.g., boron particles in rockets using boron-loaded solid propellants).

Turbulence/Particle Interactions

The problem area of greatest uncertainty in analyzing rocket plumes is the representation of turbulence processes. Turbulence processes occur in a highly compressible environment with large pressure gradients, significant chemistry, and multiphase nonequilibrium. An understanding of how these processes influence rocket plume turbulent mixing is well beyond the present state-of-the-art. Yet engineering calculations are required today which account for such effects in some rudimentary fashion.

With regard to particulates, the specific problem areas of concern are:

1) The influence of particulates on the turbulence characteristics of the gas phase (i.e., turbulence levels are diminished, the jet width is decreased, and centerline decay rates are reduced). The specific mechanisms contributing to these observed effects must be understood and turbulence models must be rationally extended based on these findings.

2) Turbulent diffusion of the particles. The rate at which particles diffuse is related to their size (the smallest particles

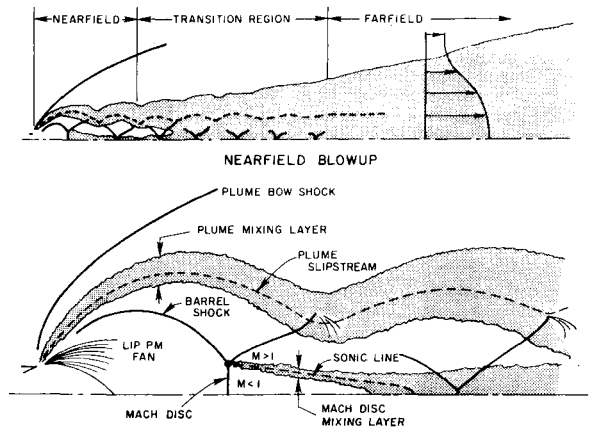

Fig. 1 Schematic of rocket exhaust plume flowfield.

Table 1 Two-phase flow interaction parameters

Parameter	Significance	$\ll 1$	~ 1	$\gg 1$
$t^* = \ell_p / L$ particle relaxation length / mean flow length scale	Indicates the ability of particles to "track" the mean flow and characterizes the magnitude of mean flow lag (i.e., differences between particle and gas phase velocities and temperatures).	*Mean flow equilibrium limit.* Particles follow the motion of the gas phase and have the same properties; equilibrated two-phase approach utilized.	*Mean flow nonequilibrium.* Particles cannot track gas and the two phases have different properties; nonequilibrium approach utilized.	*Mean flow frozen limit.* Particles have negligible influence on gas phase; phases can be treated independently in uncoupled fashion.
$t^* = t_p / t_T$ particle relaxation time / turbulence time scale	Characterizes the response of particulates to the gas phase turbulent fluctuations and hence their ability to diffuse.	*Turbulent Equilibrium Limit.* Particles respond fully to the surrounding fluctuations and diffuse like gas phase species.	*Turbulent nonequilibrium.* Particles respond partially with some degree of lag. They will diffuse differently than gas phase as characterized by their properties, the local mean flow properties and the local turbulence properties.	*Turbulent frozen limit.* Particles are not responsive to the surrounding fluctuations and do not experience any turbulent diffusion.
$\rho^* = \rho_p / \rho$ mass fraction particles / mass fraction gas	Characterizes the influence the particles have on the gas phase mean flow and turbulence.	*One way coupling.* Negligible particle loading; influence on gas phase can be neglected; one way coupling utilized for particle solution.	*Fully coupled solution.* A two-way interactive coupling between the phases is required.	*Not applicable.* This limit is *never* approached in any region of a rocket exhaust plume.

will diffuse like gaseous species, the biggest may not be influenced by the turbulence field) and other characteristics. Specific particle diffusion mechanisms must be understood and appropriate models developed. Care must be taken to distinguish between diffusive and convective motion, since both mechanisms are operative in most regions of the plume.

3) The determination of "turbulent" drag and heat transfer coefficients for high lag Mach and Reynolds numbers. The particulates are typically immersed in a highly turbulent environment which must be accounted for in establishing appropriate drag and heat transfer coefficients. The lag Mach and Reynolds numbers which occur can be quite high in regions just downstream of strong gas phase discontinuities.

Parameters Characterizing Gas/Particle/Turbulence Interactions

The overall characterization of two-phase interactions in rocket plumes is dependent on the parameters given in Table 1. These parameters must be interpreted on a local basis for each particle size group considered. Since a plume exhaust can contain particulates whose size varies by several orders of magnitude (i.e., $0.1 < r_p < 10$), it is important to make use of some of the limiting approximations to simplify the overall analysis.

Generalized Two-Phase Flow Equations

The equations governing the two-phase flow of a dilute gas/particle mixture in inviscid (nonturbulent) flow regions are well established.[1-3] The dilute assumption implies that the particulate phase occupies a negligible volume fraction of the flow and that the particles are collisionless. Thus, gas/particle coupling in inviscid flow regions is representable by forcing function terms expressing the transfer of momentum and energy between the two phases. Since rocket plume exhausts contain particulates of varying size,[4] the particulates are divided into a number of characteristic size groups, $j = 1, 2, \ldots, NP$, of fixed radius, r_{pj}, and continuum-like particle cloud equations are solved for each size group considered. The net contribution of all size groups considered is summed in evaluating the contribution of the particulates on gas phase properties.

Partially Equilibrated Two-Phase Mixture Concept

The generalized formulation presented here includes a formal equilibrium limit and expressions for turbulent particle diffusion. Via this formulation, the complete spectrum of particle to mean flow and particle to turbulent time scale ratios exhibited in Table 1 can be analyzed. In a problem encompassing particle groups of diverse size, the formulation provides for concurrent equilibrium treatment of the smaller radius particle groups and nonequilibrium treatment of the larger radius groups.

This hybrid formulation is requisite for analyzing plume exhausts, since the particle size distribution is a function of engine/propellant characteristics,[4] but is independent of the plume expansion ratio which characterizes the plume size and, hence, the mean flow length and time scales. The ratio of particle to mean flow length and time scales (which indicates the ability of particles to track the mean flow) decreases with increasing expansion ratio. Thus, at large expansion ratios a significant portion of the particulates may be effectively equilibrated with the gas phase. To avoid "stiffness" problems in the numerics in treating such near-equilibrium situations, the effectively equilibrated size groups are treated in the equilibrium limit while the remaining groups of larger particles are treated in the coupled nonequilibrium limit.

The particle/turbulence interaction formulation[5-7] requires no additional formalism to achieve the limits of particle/turbulence equilibrium (i.e., infinitely small particles; particle relaxation to turbulence time scale ratio goes to zero and particles diffuse like gas species) and frozen particle/turbulence interactions (i.e., large particle limit; particles are not responsive to turbulence fluctuations and experience no turbulent diffusion). In treating a problem encompassing a spectrum of particle sizes, both limits may be encountered, with the intermediate sized particles diffusing in accordance with the local time scale ratios, as will be discussed below.

Equilibrium Limit

In the equilibrium limit, combined gas/particle mixture equations are solved for the conservation of momentum and energy. In this limit, the dilute particle assumption plays a key role by eliminating all volumetric effects attributable to particulates. Hence the equilibrated particles exert no partial pressure and experience no pressure forces. This assumption is very reasonable one for rocket exhausts, where averaged loadings (ratio of particle flux to gas flux) rarely exceed one-half, and particulates of interest have high material densities. Under typical conditions, the particles seldom occupy more than 1% of the overall flow volume.

In stating the properties of the equilibrated mixture, the following definitions are required.

ρ_G = gas phase density
$\tilde{\rho}_p$ = particle cloud density of equilibrated particulates
$\rho_M = \rho_G + \tilde{\rho}_p$ = equilibrated mixture density
$\phi = \tilde{\rho}_p / \rho_M$ = mass fraction of equilibrated particulates

Since the particles occupy no volume, the gas phase equation of state prevails. Using the definitions above, this may be written in terms of equilibrated mixture properties as follows:

$$P = \frac{\rho_G R_0 T}{W_G} = \frac{\rho_M R_0 T}{W_M} \tag{1}$$

where the mixture molecular weight, W_M, is given by:

$$W_M = W_G / (1 - \phi) \tag{2}$$

The static enthalpy of the equilibrated mixture, h_M, is given by:

$$h_M = (1 - \phi) h_G(\alpha_i, T) + \phi h_p(T) \tag{3}$$

and thus, the specific heat capacity is given by:

$$C_{P_M} = \frac{\partial h_M}{\partial T} = (1 - \phi) C_{P_G}(\alpha_i, T) + \phi C_S(T) \tag{4}$$

In the present formulation, the particulates are all assumed to be of the same composition. Curve fits for $h_p(T)$ are incorporated which account for phase change effects (viz. solidification in the near-field expansion).

Turbulent Diffusion of Particulates

To deal with the present need for a two-phase, turbulent diffusion model for rocket plumes, an approach has been developed by Dash and Beddini[5-7] which extends concepts formulated by Melville and Bray[8] at the eddy viscosity level for use with two-equation, compressibility corrected, turbulence models presently employed for analyzing single-phase plumes.[9] In this approach, the particle diffusivity is related to that of the gas phase via a time scale relation which locally evaluates the response of the various particulate size groups to the surrounding turbulence field. The direct influence of particles on the turbulence structure is not presently accounted for. Particles will indirectly influence the turbulence field by modifying the mean gas phase velocity field via the interphase slip forcing function terms. Melville and Bray[8] have accounted for this direct influence via the use of empirical factors which yield best fits with the data. However,

their mixing model does *not* contain interphase slip forcing function terms, whose indirect influence on the mixing is substantial and cannot be neglected. In the present formulation, no empirical factors have been employed, and a single time scale constant is utilized which has *not* been formally calibrated. The calibration requires data which simulates the realm of interest for rocket plume applications (viz. particle sizes of 1-10 μm, loadings of 30%, etc.), and which clearly stipulates the initial conditions whose sensitivity for two-phase flows is pronounced (see Ref. 7). Such data is not presently available. Our present "nominal" calibration is based on incompressible jet data, which is far from the realm of interest and which does not provide the requisite initial conditions.

Particle Turbulent Transport Terms

With the particle conservation equations written in the compact form

$$\nabla \cdot (\rho_j \bar{Q}_j f_j) = S_{f_j} \tag{5}$$

where

$$f_j = \left[1, \bar{Q}_j, h_j\right]^T$$

and

$$S_{f_j} = \rho_j (f - f_j)\tau_{f_j}$$

The conventional Reynolds averaging operation yields

$$\nabla \cdot (\bar{\rho}_j \bar{Q}_j \bar{f}_j + \rho_j' Q_j' \hat{f}_j + \bar{\rho}_j Q_j' f_j') = \bar{S}_{f_j} \tag{6}$$

In arriving at this equation[7,8] third and higher order correlations are neglected; the correlation $\rho_j' f_j'$ is neglected; and mean values of the dependent variables are utilized in evaluating the forcing function term, $\bar{S}_{f_j}$. Conventional gradient hypothesis expressions are utilized for the turbulent transport terms as listed below:

$$Q_j' f_j' = -\nu_{P_j} \nabla f_j / \sigma_P \tag{7a}$$

$$\rho_j' Q_j' = -\nu_{P_j} \nabla \rho_j / \sigma_P \tag{7b}$$

Two-Phase Conservation Equations for Rocket Plumes

The partially equilibrated equations utilized for low altitude rocket plumes embody standard boundary-layer assumptions for the turbulence transport terms retained. The complete system of gas/particle equations is given in Table 2. The

Table 2 Generalized two-phase flow equations

Global mixture continuity

$$\frac{\partial}{\partial x}(r^J \rho_M U) + \frac{\partial}{\partial r}(r^J \rho_M V) = 0$$

Species continuity ($i = 1,2,\ldots,NS$)

$$\frac{\partial}{\partial x}(r^J \rho_M U \alpha_i) + \frac{\partial}{\partial r}(r^J \rho_M V \alpha_i) = \frac{\partial}{\partial r}\left(\frac{r^J}{\sigma_\alpha \rho_M \nu_M}\frac{\partial \alpha_i}{\partial r}\right) + r^J \dot{\omega}_i$$

Particle continuity ($J = 1,2,\ldots,NP$)

$$\frac{\partial}{\partial x}(r^J \rho_j u_j) + \frac{\partial}{\partial r}(r^J \rho_j v_j) = \frac{\partial}{\partial r}\left(\frac{r^J}{\sigma_P}\nu_{P_j}\frac{\partial \rho_j}{\partial r}\right)$$

Mixture streamwise momentum

$$\frac{\partial}{\partial x}(r^J [P + \rho_M U^2]) + \frac{\partial}{\partial r}(r^J \rho_M UV) = \frac{\partial}{\partial r}\left(r^J \rho_M \nu_M \frac{\partial U}{\partial r}\right) - r^J \sum_J \rho_j \frac{(U - u_j)}{\tau_{u_J}}$$

Particle streamwise momentum ($j = 1,2,\ldots,NP$)

$$\frac{\partial}{\partial x}(r^J \rho_j u_j^2) + \frac{\partial}{\partial r}(r^J \rho_j u_j v_j) = \frac{\partial}{\partial r}\left[r^J \nu_{P_j}\left(\rho_j \frac{\partial u_j}{\partial r} + \frac{u_j}{\sigma_P}\frac{\partial \rho_j}{\partial r}\right)\right] + r^J \rho_j \frac{(U - u_j)}{\tau_{u_j}}$$

Mixture normal momentum

$$\frac{\partial}{\partial x}(r^J \rho_M UV) + \frac{\partial}{\partial r}(r^J [P + \rho_M V^2]) = -r^J \sum_j \rho_j \frac{(V - v_j)}{\tau_{u_j}}$$

Particle normal momentum

$$\frac{\partial}{\partial x}(r^J \rho_j u_j v_j) + \frac{\partial}{\partial r}(r^J \rho_j v_j^2) = r^J \rho_j \frac{(V - v_j)}{\tau_{u_j}}$$

Mixture energy

$$\frac{\partial}{\partial x}(r^J \rho_M U H_M) + \frac{\partial}{\partial r}(r^J \rho_M V H_M) = \frac{\partial}{\partial r}\left(\frac{r^J \rho_M \nu_M}{\sigma_H}\frac{\partial H_M}{\partial r}\right) + \frac{\partial}{\partial r}\left[\frac{r^J \rho_M \nu_M}{\sigma_H}(\sigma_H - 1)\frac{\partial}{\partial r}\left(\frac{U^2}{2}\right)\right]$$

$$- r^J \sum_j \rho_j \left[(\bar{Q} - [\bar{Q} - \bar{Q}_j]) \cdot \frac{(\bar{Q} - \bar{Q}_j)}{\tau_{u_j}}\right] - r^J \sum_j \rho_j \frac{(h - h_j)}{\tau_{h_j}}$$

Particle energy

$$\frac{\partial}{\partial x}(r^J \rho_j u_j h_j) + \frac{\partial}{\partial r}(r^J \rho_j v_j h_j) = \frac{\partial}{\partial r}\left[\frac{r^J \nu_{P_j}}{\sigma_P}\left(\rho_j \frac{\partial h_j}{\partial r} + h_j \frac{\partial \rho_j}{\partial r}\right)\right] + r^J \rho_j \frac{(h - h_j)}{\tau_{h_j}}$$

partially equilibrated mixture equations assume that the equilibrated particulates comprising this mixture diffuse the same as the gas phase species (i.e., the small particle limit in the turbulence/particle interaction model is invoked). In addition, the particulate velocity/density correlation terms are *not* retained in the equilibrium limit to be consistent with the neglect of this correlation for the gas. This correlation is retained for the particulates in the nonequilibrium limit, yielding the turbulent transport term in the particle cloud continuity equation as well as the additional transport terms in the particle momentum and energy equations arising from their formulation in conservation form.

In Table 2, ν_M and ν_{P_j} are the mixture and particulate turbulent diffusivities. The characteristic particle times for velocity and thermal equilibration are given by

$$\tau_{u_j} = \frac{2}{9}\frac{\rho_s}{\tilde{\mu}} r_j^2 \tilde{C}_D^{-1}(Re_j, M_j) \tag{8a}$$

and

$$\tau_{h_j} = \frac{3}{2} Pr \tau_{u_j} \tilde{Nu}^{-1}(Re_j, M_j) \tag{8b}$$

Note that 1) if all particles are equilibrated with the gas, the particulate equations in Table 2 are not required and the interphase slip gas/particle forcing function terms in the mixing equations provide no contribution; while 2) if none of the particle groups are equilibrated, $\phi = 0$ and the mixture equations reduce to the nonequilibrium gas phase equations. In the general situation, the smaller particles will be treated as part of the equilibrated mixture while the larger particles will be treated by nonequilibrium procedures. The particle radius used to distinguish between equilibrated and nonequilibrated groups is problem dependent (i.e., it varies with the characteristic plume size as well as with the grid resolution; thus, the finer the grid, the smaller the particle size that can be resolved in a nonequilibrium sense) and is ascertained prior to the performance of a calculation. A more ambitious approach would involve locally splitting the particles into equilibrated or nonequilibrium groups based on the ratios of local geometric scales and particle relaxation lengths. This approach is not being pursued here.

Particle Turbulent Diffusivity

Following Melville and Bray,[8] the particle gas mixture diffusivities are related by the time scale expression:

$$\frac{\nu_{P_j}}{\nu_M} = \frac{1}{\sigma_P}\left(\frac{1}{1+\tau_{u_j}/\tau_t}\right) \tag{9}$$

where the particle Prandtl number, σ_P, is taken to be equal to that governing gas phase scalar transport (viz. $\sigma_P = \sigma_\alpha = \sigma_H$; $Le = 1$). The particle relaxation time scale, τ_{u_j}, is defined in Eq. (8a). The characteristic turbulent time scale, τ_t, is taken to be:

$$\tau_t = \frac{\Lambda}{(\overline{u'^2})^{1/2}} \tag{10}$$

where Λ is the Eulerian macrolength scale. If the gas phase is analyzed using a $k\epsilon$ type two-equation turbulence model formulation[10,11] then

$$\Lambda \sim k^{3/2}/\epsilon$$

and

$$\overline{u'^2} \sim (2/3)k$$

and, hence

$$\tau_t = C_t k/\epsilon \tag{11}$$

A nominal value of unity for the turbulence time scale constant ($C_t = 1$) appears to yield reasonable agreement with incompressible jet data. We note that the modeling approach taken here accounts for the combined effects of interphase slip and turbulent dispersion, and would appear to have capabilities comparable to those of the Stochastic Separated Flow (SSF) model of Shuen et al.[12] A second-order closure, two-phase turbulence model is now under development by Elgobashi and coworkers,[13] which accounts for the influence of particulates on the turbulence structure in a detailed fashion. However, it has been formulated from an incompressible viewpoint and thus, its extension to the highly compressible environment of rocket plumes[9,11] requires significant additional effort.

Computational Techniques

Overlaid and Fully Coupled Procedures

A variety of computational procedures have been developed for the analysis of "dilute" two-phase flow problems, as surveyed by Crowe.[14] For the analysis of rocket plume flowfields, overlaid and fully coupled types of procedures are now utilized, as reviewed in the survey paper of Dash et al.[15] In the overlaid procedure,[16] turbulent mixing and inviscid shock-capturing solutions are coupled in a weakly interactive, boundary-layer-type fashion. The overlaid procedure is valid in the plume near-field (Fig. 1) for conditions where the plume mixing layer is relatively thin (i.e., in the absence of a significant initial base/separated flow region). An extension of the overlaid procedure to analyze the base/separated flow region in the presence of an exhaust plume is now under development.[17,18] The overlaid procedure generally suffices for: engineering calculations of plume/vehicle interactions[19] where only the near-field plume solution is required; and plume infrared signatures[20] where the details of the strongly interactive plume transitional region (Fig. 1) have a negligible influence.

For plumes with large initial base/separated flow regions, the thin shear layer approximation required to use an overlaid coupling approach cannot be justified in the thick mixing layer region downstream of the reattachment point. For many types of engineering calculations, and in the interpretation of spatially resolved laboratory data, the details of the decaying shock structure in the plume transitional region (Fig. 1) are required. In such circumstances, a fully coupled numerical procedure is required to properly analyze the strongly interactive flow phenomena occurring.[21] A spatial marching, parabolized Navier-Stokes (PNS) procedure which integrates a coupled system of viscous/inviscid equations is utilized to analyze such problems.[22]

Incorporation of Two-Phase Flow Processes

The incorporation of two-phase flow capabilities into an existing single-phase flow plume model entails 1) the addition of interphase slip forcing function terms to the gas phase equations; 2) the stipulation of pertinent drag (C_D) and heat transfer (Nu) correlations; 3) the incorporation of a particle equation integration procedure; and 4) the inclusion of a particle turbulent diffusion model. The first three items were previously addressed in the development of the two-phase, inviscid shock-capturing plume model of Dash and Thorpe.[23] This model has been improved upon by: 1) the inclusion of the partially equilibrated approach discussed above (eliminating stiffness problems encountered in treating small radius particulate size groups), 2) the development of a new "floating discontinuity" limiting particle streamline approach (eliminating numerical diffusion and oscillatory problems encountered in the earlier formulation of Ref. 23 as well as in other analogous shock-capturing formulations), and 3) the development of a new approach for treating the coupled analysis of particle relaxation and turbulent mixing behind Mach disks (an item not previously addressed). These new improvements are summarized below.

The analysis of particle turbulent diffusion was originally performed by casting the particle equations into the streamfunction coordinates used to perform the gas phase turbulent mixing analysis. The details of this original formulation are available in Refs. 7 and 24. After significant numerical exploration, it was found that use of this approach was inefficient and could not account properly for the disparity in "effective jet widths" of the various particle size groups. A generalized approach for integrating the particle equations was formulated which remedies this problem and is a direct extension of the formulation in Ref. 23.

Generalized Particle Integration Procedure

A single algorithm is used to integrate the particle equations throughout the entire viscous/inviscid plume flowfield, near field and far field. With the rectangular mapping of Ref. 23 ($\xi = x$, $\eta = r/r_u$, where $r_u(x)$ is the upper boundary variation) and some algebraic manipulations, the particle equations can be cast into the following mapped vectorized form

$$\frac{\partial E_{P_j}}{\partial \xi} + \frac{\partial F_{P_j}}{\partial \eta} + G_{P_j} = \frac{b^2}{r^J}\frac{\partial}{\partial \eta}\left[r^J \nu_{P_j}\left(\rho_{P_j}\frac{\partial f_j}{\partial \eta} + f_j \frac{\partial \rho_{P_j}}{\partial \eta}\right)\right] \quad (12)$$

where

$$E_{P_j} = \rho_{P_j} u_{P_j}\{1, u_P, v_P, h_P\}_j^T$$

and

$$f_j = [1,\ u_{P_j},\ v_{P_j},\ h_{P_j}]^T$$

An upwind modification of the MacCormack algorithm (see Refs. 21 and 22) is used to integrate Eq. (12). This modification provides significant improvements in overall stability over the standard MacCormack algorithm previously used,[23] particularly in flow regions where the particle trajectories are skewed with respect to the mapped coordinate lines, $\eta = \text{const}$.

Floating Limiting Particle Streamline Approach in Inviscid Flow Regions

In the inviscid plume near-field, the limiting particle streamlines (LPS) for each particle group serve as the upper particle boundaries. In Ref. 23, the particle equations were integrated throughout the plume which tended to smear the sharp discontinuity in particle cloud density across the LPS and sometimes led to oscillatory behavior in this strong gradient region. The present approach formally traces the LPS for each group and implements a new "floating LPS" procedure which is considerably simpler to implement than procedures based on particle characteristic relations.

Referring to Fig. 2, the ξ, η mapping for the particles is the same as that used for the gas phase equations. Hence, the LPS for each group "floats" across the mapped grid points in the manner exhibited. The trajectory equation for each LPS

$$\frac{dr_{P_j}}{dx} = \frac{v_{P_j}}{u_{P_j}} \quad (13)$$

is solved and the index I_j^*, corresponding to the uppermost grid point containing particulates of size group j, is determined. Noting that the variation of u_P, v_P, and h_P along the LPS is independent of the value of ρ_{P_j}, the LPS values of ρ_{P_j} are assigned to grid points I_j^*+1 and I_j^*+2, and the particle equations are integrated to I_j^*+1 using the upwind modified MacCormack algorithm. Upon completion of this integration, the properties at the LPS position are determined via a linear interpolation, and the values of ρ_{P_j} at grid points above the LPS are set equal to zero.

This procedure yields results equivalent to a characteristic LPS procedure. The previous problems of differencing across the LPS singularity have been eliminated via the artifice of removing the singularity by smoothly extending the particle cloud density profiles across the discontinuity.

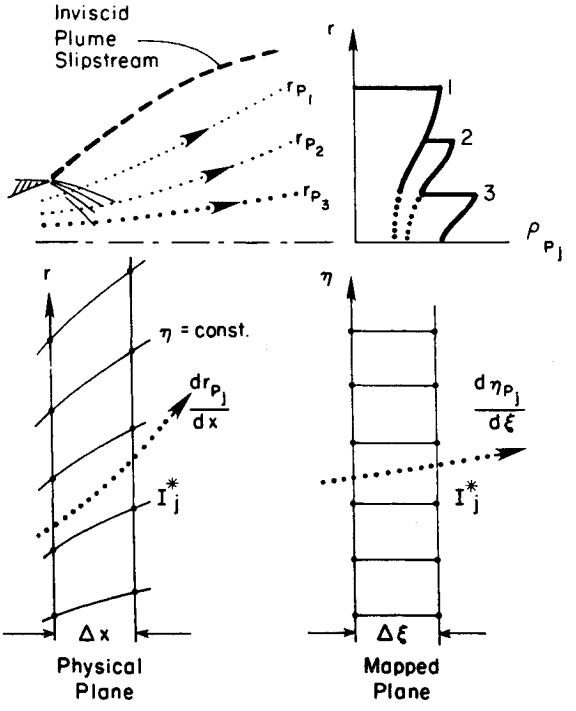

Fig. 2 Floating limiting particle streamline approach.

Particle Boundaries in Turbulent Mixing Regions

In the plume far-field, the limiting particle streamlines become dispersed by turbulent/particle diffusion and the particle cloud density varies smoothly. However, the gradients in particle cloud density can be quite severe when the LPS first enters the turbulent mixing layer and a fine grid is required to resolve these gradients. Referring to Fig. 3, the far-field analysis is performed using a separate mapping (ξ_j, η_j) for each particle group, which extends from the axis to the outer particle boundary. The axial variation of the outer boundary is defined by:

$$\frac{dr_{P_j}}{dx} = \frac{v_{P_j}}{u_{P_j}} + \frac{C r_{P_j}}{\bar{\rho}_{P_j}}\left(\frac{\partial \rho_{P_j}}{\partial r}\right)_{/\mathrm{MAX}_j} \quad (14)$$

which is analogous to the viscous/inviscid boundary growth relation used for the PNS gas phase solutions described in Refs. 21 and 22. Along the outer particle boundary, the boundary condition $\rho_{P_j} = 0$ is stipulated and the boundary relations

$$\frac{\partial u_{P_j}}{\partial \eta_j} = \frac{\partial v_{P_j}}{\partial \eta_j} = \frac{\partial h_{P_j}}{\partial \eta_j} = 0 \quad (15)$$

are enforced. Note that unlike the gas phase plume which entrains the external stream, the individual particle jets experience *no entrainment* since there are no particulates outside the r_{P_j} boundary. Hence, the particle cloud density decreases continuously with the growth of r_{P_j} brought about by the turbulent diffusion.

Mach Disk Analysis for Two-Phase Flow

Mach Disk Position

Particles will influence the Mach disk position via their effect on the shock propagation pattern and on the Mach disk streamtube solution. The first effect is straightforward to deal with while the second involves elliptic technology (i.e., up-

stream influence effects on the embedded subsonic region). For the present time, two-phase Mach disk positions are set in accordance with a sting triple-point criterion[23] which stipulates that the Mach disk be located at the position where the triple-point slipstream angle is equal to zero. This criterion does not account for upstream elliptic effects. A series of parametric calculations are described below which exhibit the dependence of the Mach disk position on the particle size using this criterion.

The calculations performed simulate an aluminized solid propellant exhaust issuing into still air with a static pressure ratio of 10/1. The nozzle exit conditions assume gas/particle equilibrium throughout the nozzle and are: $Q=9000$ ft/s (conical, 9.8 deg lip angle), $T=2000$K, and $P=3.29$ atm. The nozzle exit radius was 1 ft and the exhaust contained a 20% uniformly distributed mass loading of Al_2O_3 particulates. Parametric calculations were performed varying the particle size from 0 (equilibrium limit) to ∞ (frozen, uncoupled limit) with intermediate, nonequilibrium calculations performed for 1, 3, 10, and 100 μm radius particulates.

The trends in the plume expansion region are exhibited by the predictions of gas and particle velocities and temperatures along the centerline (from the exit plane to the Mach disk location) as shown in Fig. 4. Note that the equilibrium and frozen solutions bound the nonequilibrium solutions for gas phase variations. The particulate solutions are bound by their initial properties (frozen limit) and the equilibrium solution. In this set of runs, the 100 μm case was essentially at the frozen limit, while the 1 μm case was near the equilibrium limit.

The predicted triple-point slipstream angle variations for these runs (disk position located where $\theta_{3/4}=0$) are given in Fig. 5. The predicted variation in the Mach disk position with respect to particle size is given in Fig. 6. The position is seen to vary by about 2 jet radii between the frozen and equilibrium limits and is quite substantial. The shock jumps for the nonequilibrium solutions are all performed in the frozen limit. Note that the nonequilibrium predictions are properly bounded by the frozen and equilibrium limit solutions. The predictions clearly imply that decreasing particle size (for fixed exit plane conditions) moves the Mach disk position downstream. This trend appears to be in contradiction with the experimental observations of Lewis and Carlson.[25] They found that the Mach disk position shifted upstream as the particle size was decreased. A plausible explanation for these disparate trends is that varying the size of the particles in the experiments modified the exit plane conditions, which were held fixed in the parametric runs described here. The experimental exit plane conditions are not stipulated and, thus, meaningful comparisons cannot be performed.

Since the 1-μm case is relatively close to the equilibrium limit, the sensitivity to using equilibrated jump relations across the Mach disk was assessed for this case. Use of equilibrated jump relations boosts the pressure level behind the shock from that of the frozen calculation (see Refs. 2 and 3) and, hence, the equilibrium triple-point slipstream angle is always greater than that of the corresponding frozen angle, as exhibited by the prediction shown in Fig. 5. The disk position obtained using the equilibrated jump relations is about one jet exit radius downstream of the position obtained using frozen relations and is not bounded by the frozen equilibrium limit solutions.

The variation in relaxation length scales for the various particle size groups can be gleaned from the centerline

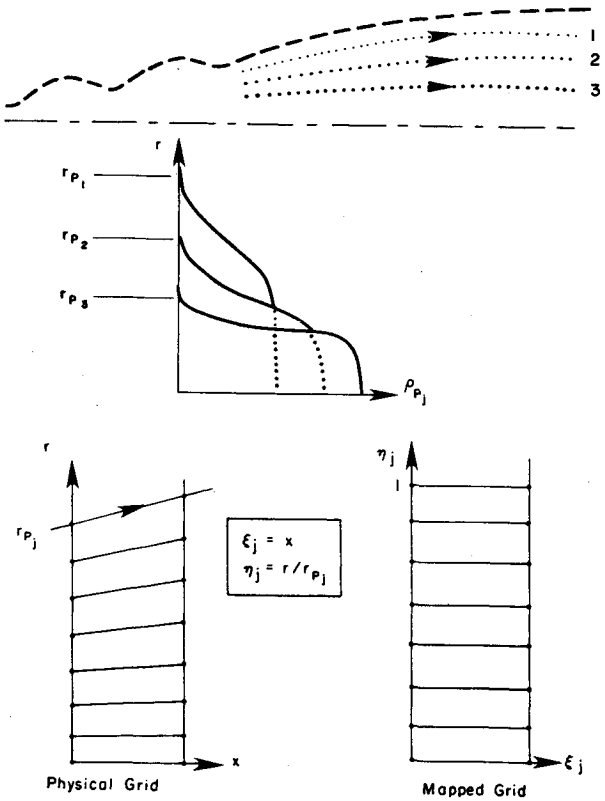

Fig. 3 Particulate far-field mapping.

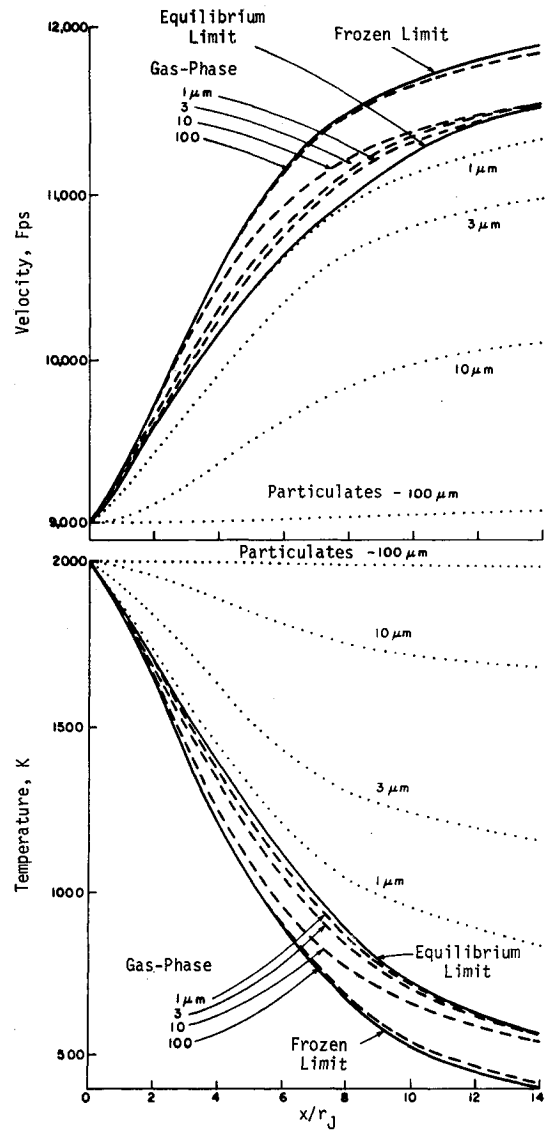

Fig. 4 Centerline variation of velocity V and temperature T in plume near-field expansion.

temperature variations plotted vs nondimensional distance from the Mach disk in Fig. 7. These are coupled relaxation predictions made using the PNS procedure to be described below. The extent of the temperature relaxation zone for the 1- and 3-μm particle cases is about 1 and 3 disk radii, respectively (the velocity relaxation lengths are about half those of the temperature), and thus not negligible with respect to characteristic dimensions of the flow. The relaxation scale for the 10-μm particles is about an order of magnitude greater than the disk radius, while that for the 100-μm particles will be more than two orders of magnitude greater. It is noteworthy that 1) the relaxation zone for the 1-μm case terminates approximately at the position of the 1-μm equilibrated Mach disk, and 2) the radius of the 1-μm equilibrated Mach disk is approximately that of the 1-μm Mach disk slipstream in the frozen case at the end of the relaxation zone (the relaxation process collapses the streamtube by increasing the gas phase velocity and decreasing the gas phase temperature). Thus, use of equilibrated Mach disk jump conditions for particles satisfying the constraint that $\ell_j/r_{MD} < 1$ appears to yield conditions which approximate those at the end of the actual relaxation zone.

Equilibrated jump relations will be required when the relaxation length scale for a particle group is so small that it becomes comparable to the numerical grid scale. However, such particle groups would ordinarily have been treated as components of the equilibrated mixture at the inception of the calculation. With this proviso, the Mach disk location should always be based on a "frozen" triple-point solution for the nonequilibrated particle groups. All particle groups treated in the plume calculation in the nonequilibrium limit will traverse the Mach disk unchanged and the relaxation process for all these groups should be formally analyzed in the coupled fashion to be discussed below.

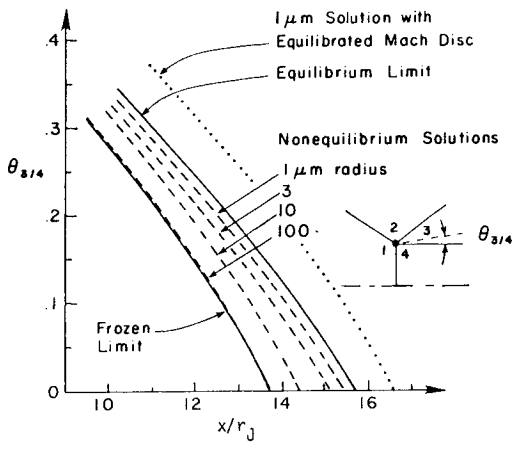

Fig. 5 Streamwise variation of triple-point slipstream angle, $\theta_{3/4}$, for various particle size groups exhibiting equilibrium and frozen bounds.

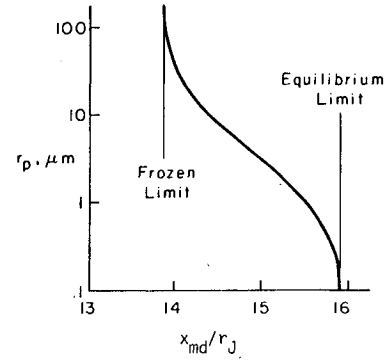

Fig. 6 Variation of Mach disk location with particle radius.

Mixing Processes Behind the Mach Disk

Experimental observations[26] and past analytical studies[27] have highlighted the important role of turbulent mixing behind the Mach disk on establishing the gas dynamic properties in the Mach disk streamtube and the size of the streamtube itself. The experiments of Back and Cuffel[26] showed the formation of a shear layer emanating from the triple point which grows rapidly into the inner stream (i.e., mixing reached the centerline in ~5 disk radii) and slowly into the outer stream (i.e., in a distance of 10 disc radii from the disk, the outer mixing layer edge is at a height of 1.4 disk radii). The nonuniform growth is due to the wakelike character of the Mach disk mixing. The mass flux per unit area of the exhaust that traverses the disk is substantially smaller than that of the exhaust just outside the Mach disk streamtube (e.g., typically a factor of 20-40). As the mixing progresses, the entrainment of the high unit mass flux outer exhaust flow into the Mach disk streamtube (or equivalently, the acceleration and cooling of the slow, hot inner stream by the faster, cooler outer stream) causes the streamtube to "collapse" (i.e., the viscous dividing streamline emanating from the triple point is displaced downward). Thus, the mixing is centered about a negatively displaced surface and hence grows non-uniformly.

Based on these observations and studies, it is quite clear that mixing must be accounted for in any model of the flow behind the Mach disk. For small disks, the mixing will reach the axis in a relatively short distance and quickly "wash away" the essentially stagnant hot temperature region prevailing there. The effect of this mixing on the pressure field for a small disk will be relatively minor since only a small volume of flow is displaced. For larger disks, a substantial volume is initially occupied by the hot, low-speed flow behind the disk; its displacement by the outer flow produces sub-

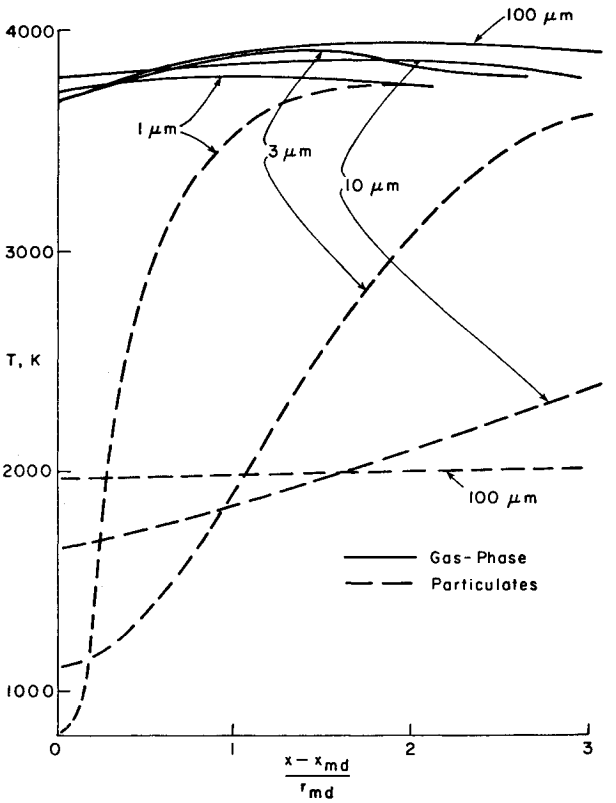

Fig. 7 Temperature relaxation process behind Mach disk for various particle sizes.

stantial negative streamline deflections which will decrease the size of the plume and affect the pressure field in a strongly interactive fashion.

Parabolized Navier-Stokes (PNS) Mach Disk Analysis

For two-phase flows, the analysis of the relaxation processes occurring behind the Mach disk must be coupled with the turbulent mixing analysis. The pressure variation along the Mach disk streamtube is arrived at by matching the inner and outer flows. A PNS model has been developed to perform the tasks of integrating the two-phase viscous/inviscid equations behind the Mach disk and coupling the inner subsonic and outer supersonic solutions. This model was specifically developed for the analysis of smaller sized Mach disk where the following assumptions can be justified: 1) the two-phase sting triple-point criterion locates the Mach disk position; 2) the extent of the subsonic region behind the disk is relatively small in comparison to inviscid flow scales; and 3) the radial pressure variation across the Mach disk streamtube is negligible.

A schematic of the flowfield behind such a Mach disk is given in Fig. 8. A sting is shown inserted into the flowfield behind the disk whose radius equals that of the Mach disk. A "porous-sting" approach[28] was first employed to perform the interactive Mach disc mixing analysis. In this approach, matching of the subsonic/supersonic streams is performed along the sting surface. The flow inside the sting is analyzed by a subsonic PNS algorithm while the flow outside the sting is analyzed by a supersonic PNS algorithm. The matching requires that the pressure imposed for the inside flow yield a sting entrainment (radial) velocity component consistent with an outer viscous-characteristic compatibility relation for the downrunning characteristic intersecting the matching point. A sublayer type approximation, in conjunction with pressure-splitting, was used to suppress elliptic "saddle-point" type behavior and thus provide direct subsonic marching capabilities. The details of this original approach are provided in Ref. 28.

To account for the variation of the sonic line and, hence, the decreasing size of the embedded subsonic region, an extension of this approach was developed whereby the inner/outer matching occurs along a mapped grid line whose index varies with the sonic line position (Fig. 8). The details of this new approach for single-phase flows are provided in Refs. 21 and 22 and sample calculations are given in Ref. 29. The numerical aspects remain the same for two-phase flows except that: the interphase slip forcing function terms contribute strongly to the overall acceleration of the gas phase, and the particles retard the rate of mixing due to lag effects (and possibly via the direct damping of the turbulent fluctuations, which is not presently accounted for).

Sample Calculation

In order to demonstrate the PNS Mach disk mixing solution with particulates of several size groups, a sample nonequilibrium prediction was performed for the representative solid propellant nozzle exhaust conditions listed in Table 3.

A second prediction was made for the gas/particle equilibrium limit. Figure 9 shows the significant differences that occur in the Mach disk solution when the full gas/particle nonequilibrium procedure is implemented. Figure 10 shows the variation of temperature along the plume centerline for both cases. While the equilibrated mixture expands to a temperature of about 1000 K and then jumps to about 4300 K behind the Mach disk (chemistry was held frozen throughout all these calculations), the gas temperature in the nonequilibrium calculation expands to about 1500 K and then jumps to about 3700 K across the disk. The 1-μm-radius particle temperatures closely follow this trend, and its relaxation zone behind the Mach disk is observed to be quite small. The other particle groups exhibit substantial lag effects with large relaxation zones. The gas phase and equilibrated mixture temperatures are noted to reach the same value at $x/r_J \sim 45$.

Two-Phase Mixing Calculations and Comparisons with Data

Aspects of Two-Phase Mixing

Experimental data for particle laden jets (see the survey by Melville and Bray[30]) indicates that 1) the particulates are dispersed by the turbulence in accordance with their response to the local turbulent fluctuations, i.e., small/light particulates will be highly responsive and diffuse like a gas phase species; large/heavy particulates will be nonresponsive and will not diffuse; and 2) the particulates can alter the rate of gas phase turbulent mixing by damping the turbulence levels and through mean flow lag effects; the net effect is a reduction in the gas phase spread rate and the rate of centerline decay.

Sample Calculations

To exhibit the operation of the particle diffusivity formulation described above and the implication of the equilibrium and frozen limits on the mixing, a series of calculations was performed for conditions representative of a sea level perfectly expanded (nonafterburning) rocket plume. Exit plane conditions were $U = 9000$ ft/s and $T = 2000$ K, with the particles starting out in equilibrium with the gas. The nozzle exit radius was 0.274 ft and the pressure was 1 atm. The mass fraction of Al_2O_3 particles was 42% and the particles were uniformly distributed across the nozzle exit plane.

The following five sets of calculations were performed:

1) Equilibrium limit calculation—all particulates treated as components of equilibrated mixture;

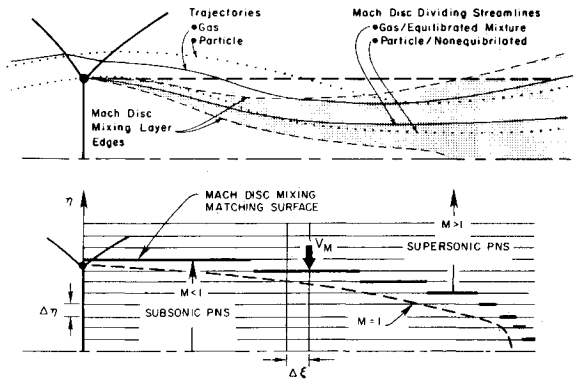

Fig. 8 Schematic of two-phase Mach disk mixing process and variable matching surface position for subsonic/supersonic PNS analysis.

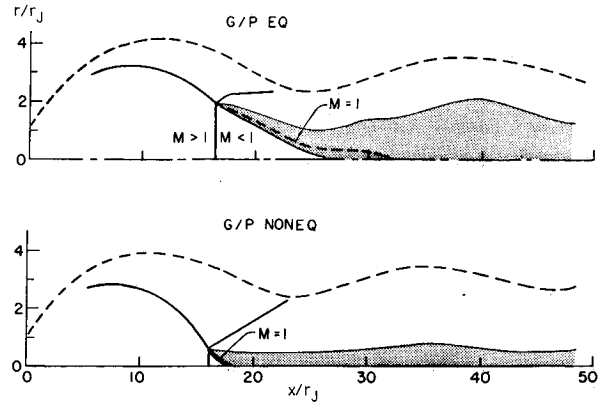

Fig. 9 Comparison of predicted near-field flow patterns for two-phase exhaust using nonequilibrium and equilibrium limit solutions.

Table 3 Sample nonequilibrium predictions

	Gas	Al_2O_3 Particulates		
		1 μm	3 μm	10 μm
U, ft/s	8700	8600	8400	8200
T, K	2300	2400	2600	2800
Particle mass fraction	—	0.14	0.14	0.14
Exit pressure, atm	8.50	—	—	—
Ambient pressure, atm	0.85	—	—	—
Exit radius, ft	0.25	—	—	—

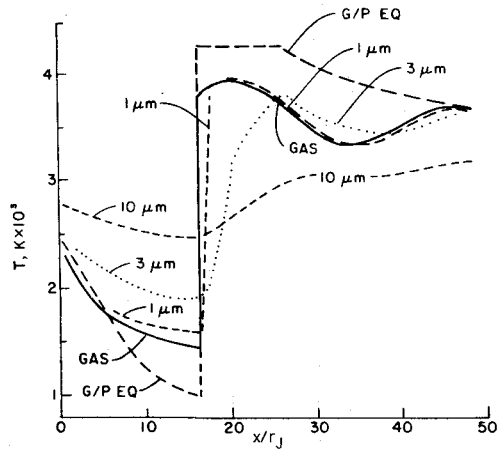

Fig. 10 Comparison of gas/particle temperature variations along plume centerline.

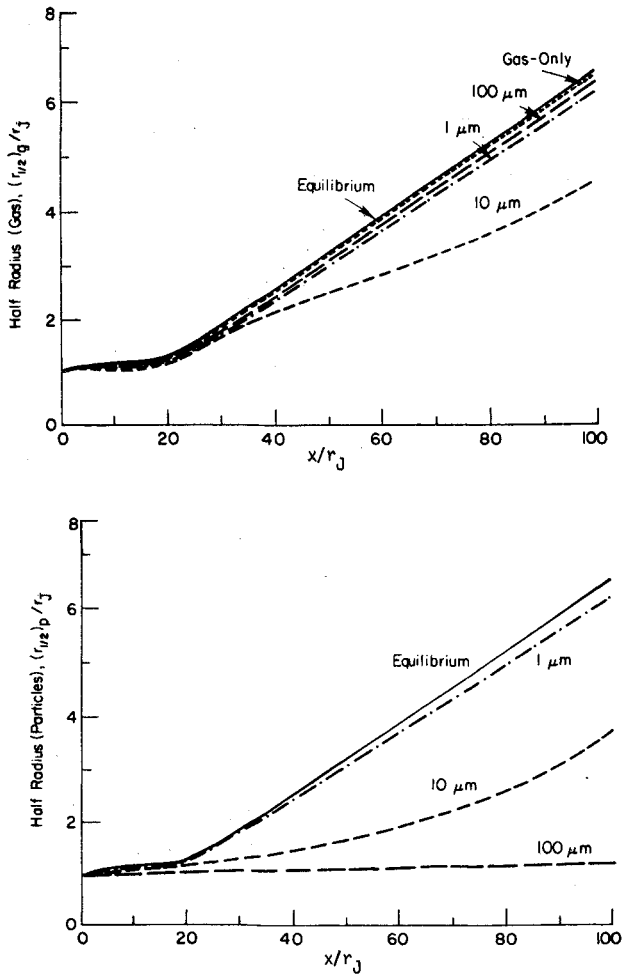

Fig. 11 Effect of particle size on gas and particle jet spread.

2) Nonequilibrium calculation—all particulates have 1-μm radius;

3) Nonequilibrium calculation—all particulates have 10-μm radius;

4) Nonequilibrium calculation—all particulates have 100-μm radius;

5) Frozen limit calculation—gas phase solution obtained without particulate interactions.

Figure 11 shows the gas and particle spread rates. Only the 10-μm particles have an appreciable influence on the spread rate of the gas. The 1-μm particles are nearly in equilibrium with the gas (as indicated by the comparison of the nonequilibrium 1-μm solution with the formal equilibrium solution) while the 100-μm particles have no effect on the gas (as indicated by the comparison of the frozen gas-only solution with the nonequilibrium 100-μm solution). Figure 12 depicts the centerline velocity decays for the above calculations. The centerline decay for the gas phase in the frozen limit is the most rapid. The 100-μm calculation was essentially at the frozen limit, as evidenced by no significant change in the 100-μm particle velocities from the initial conditions and, hence, the same gas phase decay as in the formal frozen limit. The particulates have a significant influence on the gas phase velocity decay as evidenced by the equilibrium limit solution. Here, the inviscid core length is shifted downstream by about 3 jet radii and the distance required to decay to 1/4 the initial velocity is shifted downstream by about 8 jet radii. The 1-μm calculation is essentially at the equilibrium limit—the gas phase and equilibrium solu-

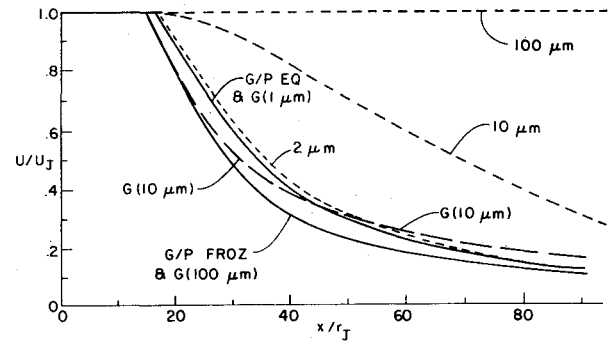

Fig. 12 Influence of particle size on velocity decay.

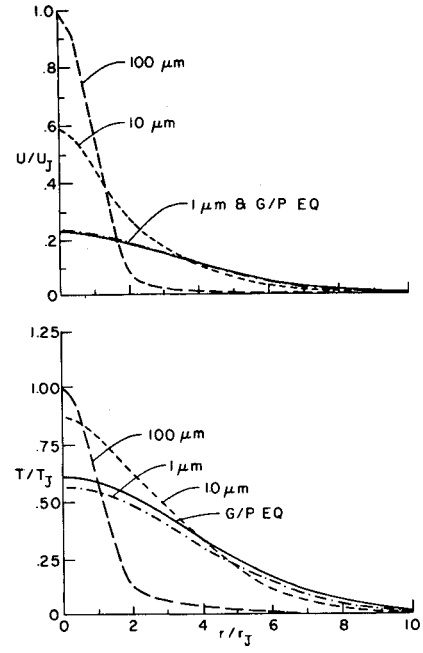

Fig. 13 Velocity and temperature profiles at $x/r_J = 60$.

tions coincide and the departure of the 1-μm particulate solution from the equilibrium limit solution is too small to plot on this scale. A 2-μm particle solution has slight departures, as exhibited in Fig. 12. The 10-μm solution is well out of equilibrium; the gas phase 10-μm solution starts on the frozen branch and overshoots the equilibrium limit. The 10-μm particle solution sits well above the equilibrium limit solution. The two solutions start to closely approach the equilibrium limit solution and should coincide with it for $x/r_J > 100$.

Profiles of particle velocity and temperature at $x/r_J = 60$ (Fig. 13) indicate the extent of the particulate mixing region in comparison to that of the equilibrated mixture. The 1-μm particles have essentially dispersed like the gaseous phase while the 100-μm particulates have experienced very little turbulent diffusion. Further details of these calculations are given in Ref. 24.

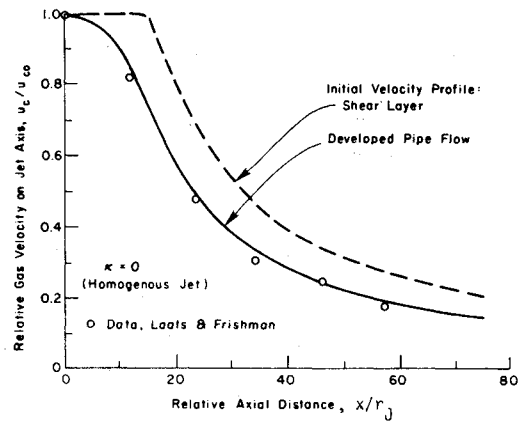

Fig. 14 Homogeneous jet solution; influence of initial profile.

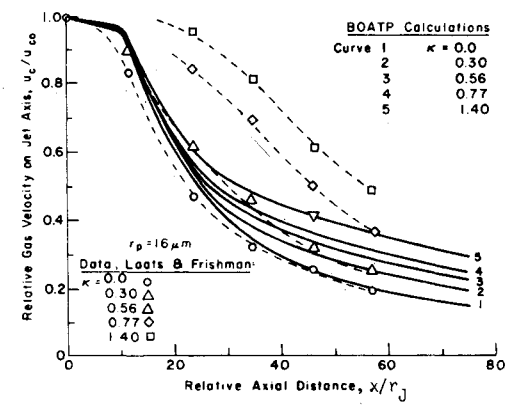

Fig. 15 Effect of particle loading on gas phase velocity decay.

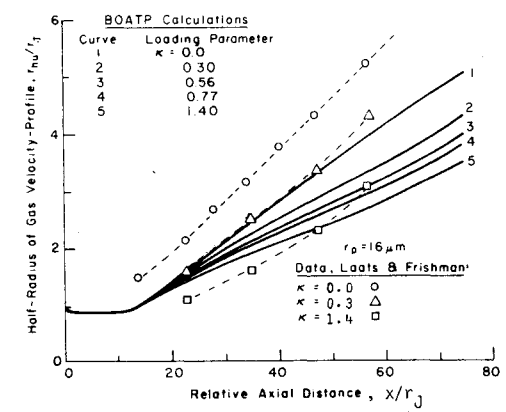

Fig. 16 Effect of particle loading on gas phase half-radius variation.

Analysis of Laats and Frishman Data

An evaluation of available experimental data for particle dispersion in turbulent jets led to the selection of the Laats and Frishman[31,32] results which were obtained using corundum (Al_2O_3) particles in air, and cover a broad range of particle radii ($8.5 \le r_P \le 40$ μm) and initial particulate mass loading ratios ($0 \le \kappa \le 1.4$). Some potentially important experimental information was not reported (viz. the initial conditions) which introduces considerable uncertainty in simulating the flow. An attempt to assess the influence of the initial conditions parametrically in the analysis has been made.

The experimental jet issued from a straight pipe of internal radius $r_J = 1.75$ cm; the jet exit profiles were not reported. It is assumed that a partially developed pipe flow exists at the jet exit, with the axial velocity profile specified by $u/u_{co} = (1 - r/r_J)^{0.2}$ and faired into a thin shear layer about $r = r_J$. Use of this type of profile as a computational initial condition yields good agreement with the decay of axial velocity on the jet axis for the homogeneous (no particulates) baseline calculation, as shown by the solid line in Fig. 14. To demonstrate the sensitivity to the assumed initial velocity profile, a calculation was also performed with a top hat profile. This produces a conventional inviscid core approximately $18r_J$ in length, and appreciably displaces the calculated velocity decay curve (dashed line) away from the data. The developed power law profile was therefore employed for gas and particulate axial velocity profiles in subsequent calculations.

The density loading parameter κ (defined by ρ_j/ρ at $x = 0$ and $r = 0$ for initially equilibrated particulates) was varied from 0 to 1.4 for a fixed particle radius, $r_p = 16$ μm. Both data and calculations (Fig. 15) display a decrease in the decay rate of axial velocity as the particulate loading is increased. The observed effect is more pronounced than that predicted, especially within $x/r_J \le 40$. This has been interpreted[30,31] to be a gross indication of an appreciable reduction in gas phase turbulence levels as particulate loading is increased, which is not accounted for in the present model. Note that the result at the lightest loading (curve 2) agrees reasonably well with the data for $x/r_J > 40$ and is the only loading representative of that in a rocket plume. The initial experimental behavior appears to indicate conditions which are also not accounted for in the predictions.

The effect of κ on the spread of the gas phase axial velocity profile is shown in Fig. 16 for a constant particle size of $r_p = 16$ μm. The parameter r_{hu} is the half-radius of the gas velocity profile. The calculated results given by the curves 1 through 5 show that there is an appreciable decrease in the gas phase spread rate in the region $20 \le x/r_J \le 60$ as κ is increased from 0 to 1.4. Beyond $x/r_J = 60$, the behavior of r_{hu} for $\kappa \ne 0$ tends toward the homogeneous jet spread rate. Similar qualitative behavior is evident in the experimental data. However, the data additionally show a pronounced effect of particulate loading on spread rates in the initial region ($0 \le x/r_J \le 20$) which is not displayed by the calculations.

Laats and Frishman measured the mean axial particulate mass flux $g_p = \rho_p u_p$ at several axial and radial positions. The relative axial decay of g_p on the centerline (g_{pc}/g_{pco}) is shown in Fig. 17 for $\kappa = 0.3$ and various particle sizes. The data is anomalous (with respect to the classical decay of gaseous species) in the appearance of a pronounced maximum in the region $x/r_J < 25$ for smaller particle sizes. The calculated results obtained with the nominal initial conditions stated previously are shown as curves 1, 3, and 4 for particle sizes of $r_p = 8.5$, 16, and 40 μm, respectively. These results may be considered physically intuitive in that they show an appreciable decrease in the decay rate as particle size is increased.

In considering the near-field maximum in experimental data, it appeared possible that this phenomenon arose from a

radially inward convection velocity initially exceeding the outward effective diffusion velocity of the particulates. A possible physical mechanism for achieving this is the rapid entrainment of the gas near the nozzle (pipe) lip due to relaxation of the exit profiles. To account for this type of effect, particles in the lip region were given a small negative radial velocity of $v_{p,\max}/u_{co} = -0.05$ for the $r_p = 8.5$ μm particle group. The result of this calculation is shown by curve 2 in Fig. 17, which achieves a near-field maximum comparable to the corresponding data. It was also found that decreasing $v_{p,\max}/c_{co}$ to -0.10 increased the centerline mass flux maximum to 1.67, thus indicating the sensitivity of initial radial convection effects on downstream particulate behavior. The value of $v_{p,\max}/u_{co} = -0.05$ is not regarded as unreasonable with respect to gas phase entrainment velocities in the exit region, and smaller particles would be more susceptible to this effect.

With respect to the larger particles ($r_p = 40$ μm), curve 5 in Fig. 17 was obtained with a positive (divergent) radial velocity of $v_{p,\max}/u_{co} = 0.05$ and is much more representative of the experimental data than curve 4. This source-like divergent behavior for larger particles could be due to their release from a point (viz. a small central pipe) within the duct.

The effect of particle size on the behavior of the half-radius of particulate mass flux r_{hg} is shown in Fig. 18 for $\kappa = 0.3$. (The calculated results given by curves 1, 2, and 3 correspond with the nominal conditions stated for curves 1, 3, and 4 in Fig. 17.) The calculations indicate a monotonic and significant decrease in spread rate with increasing particle size, the larger particle size group displaying almost negligible dispersion. The experimental results do not show an appreciable effect of particle size and are nonmonotonic, although the physically anticipated particle size trend is displayed in the far field.

Further details of this data analysis are reported in Ref. 7.

JANNAF Standard Plume Flowfield (SPF) Model

Over the past several years, the authors and coworkers have been engaged in the development of the JANNAF (Joint Army, Navy, NASA, Air Force) Standard Plume Flowfield (SPF) Model, a computer code which will be the U.S. government and industry standard for predicting the gas dynamic structure of single- and two-phase low-altitude (<70 km) rocket exhaust plumes. The SPF treats single nozzle

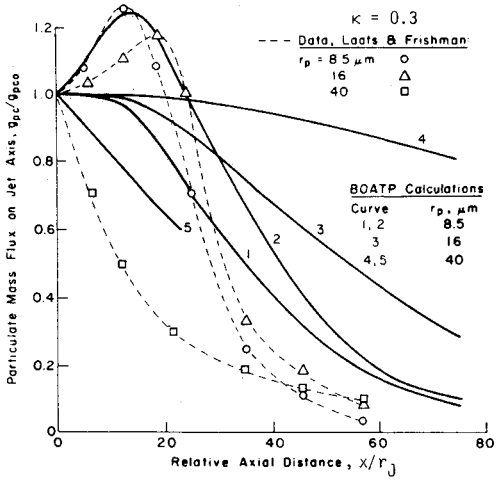

Fig. 17 Effect of particle size on particulate mass flux decay.

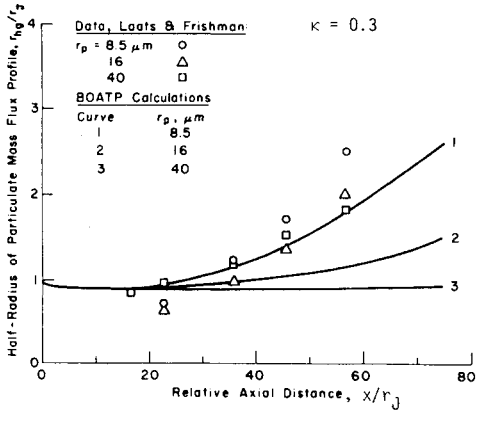

Fig. 18 Effect of particle size on particulate dispersion.

Table 4 Versions of JANNAF SPF

Version	Near field	Transition region	Far field	Key features/limitations
SPF/1	Mixing overlaid on inviscid map	Mixing with prescribed pressure decay	Constant pressure mixing	Single-phase flow No Mach disk mixing/chemistry Uniform composition exhaust Finite rate chemistry in mixing solution Initial plume expansion angle ≤70 deg.
SPF/2	Plume mixing layer overlaid on viscous/inviscid map containing Mach disk mixing solution	As above; plume and Mach disk mixing layers merged	Constant pressure mixing	Single- and two-phase flow Mach disk mixing Uniform composition exhaust Finite rate and equilibrium chemistry options in mixing solution Initial plume expansion angle >90 deg.
SPF/3	Fully coupled parabolized Navier-Stokes solution		Constant pressure mixing	Single- and two-phase flow Mach disk mixing/chemistry Nonuniform composition exhaust Finite rate and equilibrium chemistry options throughout the plume Initial plume expansion angle >90 deg

exhausts at zero angle of attack and presently excludes the effects of missile base flows and plume-induced separation. The SPF is intended for use in a number of problem areas, the principal applications being the prediction of plume signatures and plume/vehicle interaction phenomena.

Table 4 summarizes features of three versions of the SPF. Both SPF/1 and SPF/2 combine a near-field overlaid approach with a far-field pressure-equilibrated approach, while SPF/3 models the near-field with a fully coupled viscous/inviscid parabolized Navier-Stokes solution. The methodology employed in SPF/2 gives significantly enhanced capabilities over SPF/1, principally in the treatment of particulates. SPF/1 was written for single-phase or gas/particle equilibrium flow, while SPF/2 accounts for full gas/particle nonequilibrium effects in the inviscid plume and transitional and far-field mixing regions using the methodology described in this article. Another major area of increased capabilities concerns the treatment of the flow downstream of the Mach disk. In SPF/2, the parabolized Navier-Stokes methodology discussed in this article has been incorporated to treat the subsonic/supersonic turbulent mixing process in this region. The capabilities of SPF will be further expanded with SPF/3 to account for full coupling between the inviscid/shock and viscous solutions.

SPF/1 was made available to industry in 1981. The computational methodology employed and the operational aspects of the code have been described in several publications.[33-36] A preliminary version of SPF/2 is presently operational whose detailed description and results for two-phase, afterburning plumes are given in Ref. 37. The key numerical features of the fully coupled parabolized Navier-Stokes approach employed in SPF/3 are described in Refs. 21, 22, and 37-39. This model is presently under development.

Concluding Remarks

Aspects of two-phase flow processes in rocket plumes were reviewed. An approach for analyzing the complete spectrum of particle sizes encounterable in rocket plumes was presented which treats the smallest particles (those whose equilibration lengths are comparable to the grid size) in the equilibrium limit and all others in nonequilibrium. Numerical studies were performed which exhibit the dependence of flow parameters on particle size and demonstrate the bounding qualities provided by the frozen ($r_p \to \infty$) and equilibrium ($r_p \to 0$) limits.

The dependence of the Mach disk position on particle size was ascertained. For fixed exit plane properties, decreasing the particle size moves the Mach disk position downstream. The equilibrium and frozen solutions provide the limiting positions of the disk. It was shown that the location of the disk must be based on shock relations which freeze the particle properties in traversing the shock front. The gas/particle relaxation process behind the disk was shown to occur over a length scale which (generally) cannot be ignored in comparison to the Mach disk radius. As such, the relaxation process is strongly coupled to the other gas dynamic processes occurring in the Mach disk streamtube. A parabolized Navier-Stokes Mach disk model was presented which calculates these coupled processes using a sublayer approximation to eliminate elliptic (upstream influence) effects. Results were presented to exhibit the performance of this model in plumes with small to moderate radius Mach disks. For larger disks, an iterative elliptic procedure is necessary to analyze this problem.

The preliminary theoretical model developed for particle dispersion in turbulent jets has been shown to yield qualitative and, in specific cases, quantitative agreement with experimental trends. Over the particle size and initial mass loading ranges considered in comparisons with the Laats and Frishman data, the model was found to be in agreement with the following macroscopic trends:

1) An increase in particulate loading decreases both gas and particulate phase mixing (dispersion) rates at constant particle size.

2) An increase in particle size at a constant and moderate level of initial loading decreases particulate dispersion.

3) The effects of initial (jet exit) conditions are theoretically indicated to be quite important in the calculation of downstream two-phase flow development. In particular, it is found that relatively low values of initial particulate radial velocity theoretically can rationalize the pronounced near-field overshoot in particulate mass flux observed by Laats and Frishman. Inclusion of the radial particulate momentum equation in the present formulation has thus been essential; its neglect in previous models casts doubts on their use in interpretation of these data.

Further theoretical research is required on the particle-turbulence interaction aspects of the overall jet mixing problem. The present formulation neglects the direct effects of particulates on gas phase turbulence. As a consequence, turbulent energy transfer between phases is not conserved, although this microscopic transfer process governs macroscopic behavior of more practical interest. A possible approach to the problem would involve treating the dynamics of turbulence for each phase in a coupled manner, following Reynolds decomposition of the governing equations, rather than introduction of Boussinesq approximations at the outset. The results of the present analysis indicate that particle inertial effects may be responsible for some phenomena which have been predominantly attributed to particle turbulent interactions in prior studies.

It will also be necessary to obtain more detailed experimental measurements of multiphase turbulent jet flows, and for application to rocket plumes, data on supersonic flows are required.An objective of the Laats and Frishman experiment was to provide mean flow data for a broad range of particle sizes and mass loadings. This objective could be extended with newer (e.g., optical) diagnostic techniques to obtain the data on gas and particulate turbulence characteristics required for detailed and unambiguous model validation. Particular attention should be given to flow measurements near to and upstream of the jet exit.

References

[1] Soo, S. I., *Fluid Dynamics of Multiphase Systems,* Blaisdell Pub. Co., Waltham, Mass., 1967.

[2] Marble, F. E., "Dynamics of Dusty Gases," *Annual Review of Fluid Mechanics,* Annual Reviews, Inc., Palo Alto, Calif., 1970, pp. 397-446.

[3] Rudinger, G., "Relaxation in Gas-Particle Flow," *Nonequilibrium Flows, Part I,* Marcel Dekker, Inc., New York, 1969, pp. 119-161.

[4] Hermsen, R. W., "Aluminum Oxide Particle Size for Solid Rocket Motor Performance Prediction," *Journal of Spacecraft and Rockets,* Vol. 18, Nov.-Dec. 1981, pp. 483-490.

[5] Dash, S. M., "Computational Methodology for the Inclusion of Gas/Particle Nonequilibrium Effects in Exhaust Flowfields," *JANNAF 12th Plume Technology Meeting,* CPIA Pub. 332, Vol. II, Dec. 1980, pp. 289-350.

[6] Dash, S. M., "Gas Particle Interactions in Rocket Exhaust Plumes," *Multiphase Flows,* edited by D. A. Drew, *Proceedings of ARO International Workshop at BRL,* Feb. 1980, pp. 17-40.

[7] Beddini, R. A. and Dash, S. M., "Turbulent Mixing Analysis of Particle Laden Jets," *JANNAF 13th Plume Technology Meeting,* CPIA Pub. 357, Vol. II, April 1982, pp. 127-142.

[8] Melville, W. K. and Bray, K. N. C., "A Model of the Two-Phase Turbulent Jet," *International Journal on Heat and Mass Transfer,* Vol. 22, 1979, pp. 647-655.

[9] Pergament, H. S., "Assessment and Recommendation of Two-Equation Turbulence Models for Rocket and Aircraft Plume Flowfield Predictions," NWC TP 6364, July 1982 (also *JANNAF 13th Plume Technology Meeting,* CPIA Pub. 357, Vol. II, April 1982, pp. 73-126).

[10] Launder, B. E., Morse, A., Spalding, D. B., and Rodi, W., "Prediction of Free Shear Flows: A Comparison of Six Turbulence Models," *Free Turbulent Shear Flows, Vol. I,* NASA SP-321, 1972, pp. 361-426.

[11] Dash, S. M., Weilerstein, G., and Vaglio-Laurin, R., "Compressibility Effects in Free Turbulent Shear Flows," AFOSR-TR-75-1436, Aug. 1975.

[12] Shuen, J. S., Solomon, A. S. P., Zhang, Q. F., and Faeth, G. M., "The Structure of Particle-Laden Jets and Nonevaporating Sprays," NASA CR-168059, Feb. 1983.

[13] Elghobashi, S. E. and Rizk, M. A., "Effect of Solid Particles on the Turbulent Flow of a Round Gaseous Jet," Dept. of Energy Report DE 84-005830, 1984.

[14] Crowe, C. T., "Numerical Models for Dilute Gas-Particle Flows," *ASME Journal of Fluids Engineering,* Vol. 104, Sept. 1982, pp. 297-303.

[15] Dash, S. M., Pergament, H. S., and Wolf, D. E., "Computation of Viscous/Inviscid Interactions in Exhaust Plume Flowfields, Part I: Overlaid and Fully-Coupled Methodology," *Symposium on Rocket/Plume Fluid Dynamic Interactions,* Huntsville, Ala., April 1983 (U.S. Army Research Office, Fluid Dynamics Labs., Rept. 83-104, Vol. I).

[16] Dash, S. M., Wilmoth, R. G., and Pergament, H. S., "An Overlaid Viscous/Inviscid Model for the Prediction of Nearfield Jet Entrainment," *AIAA Journal,* Vol. 17, Sept. 1979, pp. 950-958.

[17] Dash, S. M. and Sinha, N., "Computation of Viscous/Inviscid Interactions in Exhaust Plume Flowfields, Part II: Overlaid Approach for Supersonic Base Flow Analysis," *Symposium on Rocket/Plume Fluid Dynamic Interactions,* Huntsville, Ala., April 1983 (U.S. Army Research Office, Fluid Dynamics Labs., Rept. 83-104, Vol. I).

[18] Dash, S. M. and Sinha, N., "Overlaid Component Model for Base Region Analysis of Rocket Plumes at Supersonic Flight Velocities," *JANNAF 14th Plume Technology Meeting*, CPIA Pub. 384, Vol. II, Nov. 1983, pp. 227-252.

[19] Wilmoth, R. G., "Aerodynamic Interactions with Turbulent Jet Exhaust Plumes," *JANNAF 13th Plume Technology Meeting,* CPIA Pub. 357, Vol. I, April 1982, pp. 315-330.

[20] Dash, S. M., Pearce, B. E., Pergament, H. S., and Fishburne, E. S., "Prediction of Rocket Plume Flowfields for Infrared Signature Studies," *Journal of Spacecraft and Rockets,* Vol. 17, May-June 1980, pp. 190-199.

[21] Dash, S. M. and Wolf, D. E., "Interactive Phenomena in Supersonic Jet Mixing Problems, Part I: Phenomenology and Numerical Modeling Techniques," *AIAA Journal*, Vol. 22, July 1984, pp. 905-913.

[22] Dash, S. M. and Wolf, D. E., "Fully-Coupled Analysis of Jet Mixing Problems, Part I: Shock-Capturing Model, SCIPVIS," NASA CR 3761, Jan. 1984.

[23] Dash, S. M and Thorpe, R. D., "Shock-Capturing Model for One- and Two-Phase Supersonic Exhaust Flows," *AIAA Journal,* Vol. 19, July 1981, pp. 842-851.

[24] Beddini, R. A., Dash, S. M., and Pergament, H. S., "Numerical Investigation and Parametric Analysis of Gas/Particle Interactions in a High Speed Mixing Region," TM-16, Science Applications, Inc., Princeton, N.J., Nov. 1982.

[25] Lewis, Jr., C. H. and Carlson, D. J., "Normal Shock Location in Underexpanded Gas and Gas-Particle Jets," *AIAA Journal,* Vol. 2, April 1964, pp. 776-777.

[26] Back, L. H. and Cuffel, R. B., "Viscous Slipstream Flow Downstream of a Centerline Mach Reflection," *AIAA Journal,* Vol. 9, Oct. 1971, pp. 2107-2109.

[27] Dash, S. M. and Pergament, H. S., "A Computational System for the Analysis of Mixing/Chemical/Shock Processes in Supersonic Internal and Exhaust Plume Flowfields," AIAA Paper 80-1255, Hartford, Conn., June/July 1980.

[28] Dash, S. M. and Wolf, D. E., "Advances in Two-Phase Flow Modeling for the JANNAF Standard Plume Flowfield Model," *JANNAF 13th Plume Technology Meeting*, CPIA Pub. 357, Vol. II, April 1982, pp. 41-72.

[29] Dash, S. M. and Wolf, D. E., "Interactive Phenomena in Supersonic Jet Mixing Problems, Part II: Numerical Studies," to be published in *AIAA Journal.*

[30] Melville, W. K. and Bray, K. N. C., "The Two-Phase Turbulent Jet," *International Journal on Heat and Mass Transfer,* Vol. 22, 1979, pp. 279-287.

[31] Laats, M. K. and Frishman, F. A., "Assumptions Used in Calculating the Two-Phase Jet," *Mekhanica Zhidkosti i Gaza,* Vol. 5, Feb. 1970, pp. 186-191.

[32] Laats, M. K. and Frishman, F. A., "Scattering of an Inert Admixture of Different Grain Size in a Two-Phase Axisymmetric Jet," *Heat Transfer-Soviet Research,* Vol. 2, 1970, pp. 7-11.

[33] Dash, S. M., Pergament, H. S., and Thorpe, R. D., "The JANNAF Standard Plume Flowfield Model—Modular Approach and Preliminary Results," *JANNAF 11th Plume Technology Meeting,* CPIA Pub. 306, Vol. I, July 1979, pp. 345-442.

[34] Dash, S. M. and Pergament, H. S., "The JANNAF Standard Plume Flowfield Model: Operational Features and Preliminary Assessment," *JANNAF 12th Plume Technology Meeting,* CPIA Pub. 332, Vol. II, Dec. 1980, pp. 225-288.

[35] Dash, S. M. and Pergament, H. S., "The JANNAF Standard Plume Flowfield Model (SPF)," Army Missile Command, Huntsville, Ala., TR RD-CR-82-9, April 1981.

[36] Dash, S. M. and Pergament, H. S., "The JANNAF Standard Plume Flowfield Model (SPF)—Program Users Guide for Interim Version (SPF/1)," Army Missile Command, Huntsville, Ala., Special Report RD-81-4, July 1981.

[37] Dash, S. M., Pergament, H. S., and Wolf, D. E., "Overlaid and Fully-Coupled Versions of the JANNAF Standard Plume Flowfield Model (SPF/2 and SPF/3)," *JANNAF 14th Plume Technology Meeting,* CPIA Pub. 384, Vol. II, Nov. 1983, pp. 169-226.

[38] Dash, S. M. and Wolf, D. E., "Development of Fully-Coupled Viscous/Inviscid Technology for the Analysis of Exhaust Plume Flowfields," *JANNAF 13th Plume Technology Meeting,* CPIA Pub. 357, Vol. I, April 1982, pp. 115-182.

[39] Dash, S. M. and Wolf, D. E., "Shock-Capturing Parabolized Navier-Stokes Model (SCIPVIS) for the Analysis of Turbulent Underexpanded Jets," AIAA Paper 83-0704, Atlanta, Ga., April 1983.